Inter-subject pattern analysis A straightforward and powerful scheme for group-level MVPA

Qi Wang, Bastien Cagna, Thierry Chaminade, Sylvain Takerkart

Inter-subject pattern analysis
A straightforward and powerful scheme for group-level MVPA

Qi Wang[a,b], Bastien Cagna[a], Thierry Chaminade[a], Sylvain Takerkart[⋆a]

⋆ *Corresponding author: Sylvain.Takerkart@univ-amu.fr*

https://doi.org/10.1016/j.neuroimage.2019.116205

[a] *Institut de Neurosciences de la Timone UMR 7289, Aix-Marseille Université, CNRS*
Faculté de Médecine, 27 boulevard Jean Moulin, 13005 Marseille, France
[b] *Laboratoire d'Informatique et Systèmes UMR 7020, Aix-Marseille Université, CNRS, Ecole Centrale de Marseille*
Faculté des Sciences, 163 avenue de Luminy, Case 901, 13009 Marseille, France

Abstract

Multivariate pattern analysis (MVPA) has become vastly popular for analyzing functional neuroimaging data. At the group level, two main strategies are used in the literature. The standard one is hierarchical, combining the outcomes of within-subject decoding results in a second-level analysis. The alternative one, inter-subject pattern analysis, directly works at the group-level by using, e.g. a leave-one-subject-out cross-validation. This study provides a thorough comparison of these two group-level decoding schemes, using both a large number of artificial datasets where the size of the multivariate effect and the amount of inter-individual variability are parametrically controlled, as well as two real fMRI datasets comprising 15 and 39 subjects, respectively. We show that these two strategies uncover distinct significant regions with partial overlap, and that inter-subject pattern analysis is able to detect smaller effects and to facilitate the interpretation. The core source code and data are openly available, allowing to fully reproduce most of these results.

Keywords: fMRI, MVPA, group analysis

1. Introduction

Over the past decade, multi-voxel pattern analysis (MVPA, [15]) has become a very popular tool to extract knowledge from functional neuroimaging data. The advent of MVPA has offered new opportunities to examine neural coding at the macroscopic level, by making explicitly usable the information that lies in the differential modulations of brain activation across multiple locations – i.e. multiple sensors for EEG and MEG, or multiple voxels for functional MRI (fMRI). Multivariate pattern analysis commonly consists in *decoding* the multivariate information contained in functional patterns using a classifier that aims to guess the nature of the cognitive task performed by the participant when a given functional pattern was recorded. The decoding performance is consequently used to measure the ability of the classifier to distinguish patterns associated with the different tasks included in the paradigm. It provides an estimate of the *quantity of information* encoded in these patterns, which can then be exploited to localize such informative patterns and/or to gain insights on the underlying cognitive processes involved in these tasks.

This decoding performance is classically estimated separately in each of the participants. At the group level, these within-subject measurements are then combined – often using a *t*-test – to provide population-based inference, similarly to what is done in the standard hierarchical approach used in activation studies. Despite several criticisms of this group-level strategy that have been raised in the literature (see herafter for details), this hierarchical strategy remains widely used.

An alternative strategy directly works at the group-level by exploiting data from all available individuals in a single analysis. In this case, the decoding performance is assessed on data from new participants, i.e. participants who did not provide data for the training of the classifier (see e.g. [32, 17, 19, 20, 18, 10]), ensuring that the *nature of the information* is consistent across all individuals of the population that was sampled for the experiment. This strategy takes several denominations in the literature such as across-, between- or inter-subject classification or subject-transfer decoding. We hereafter retain the name inter-subject pattern analysis (ISPA).

In this paper, we describe a comparison of the results provided by these two classifier-based group-level decoding strategies with both artificial and real fMRI datasets, which, to the best of our knowledge, is the first of its kind. This experimental study was carefully designed to exclusively focus on the differences induced by the within- vs. inter-subject nature of the decoding, i.e. by making all other steps of the analysis workflow strictly identical. We provide results for both two real fMRI datasets and a large number of artificial datasets where the characteristics of the data are parametrically controlled. This allows us to demonstrate that these strategies offer different detection power, with a clear advantage for the inter-subject scheme, but furthermore that they can provide results of different nature, for which we put forward a potential explanation supported by the results of our simulations on artificial data. The paper is orga-

nized as follows. Section 2 describes our methodology, including our multivariate analysis pipeline for the two group-level strategies, as well as a description of the real datasets and the generative model of the artificial datasets. Section 3 includes the comparison of the results obtained with both strategies on these data, both in a qualitative and quantitative way. Finally, in Section 4, we discuss the practical consequences of our results and formulate recommendations for group-level MVPA.

2. Methods

2.1. Group-MVPA (G-MVPA)

Since the seminal work of [16] that marked the advent of multivariate pattern analysis, most MVPA studies have relied on a within-subject decoding paradigm. For a given subject, the data is split between a training and a test set, a classifier is learnt on the training set and its generalization performance – usually measured as the classification accuracy – is assessed on the test set. If this accuracy turns out to be above chance level, it means that the algorithm has identified a combination of features in the data that distinguishes the functional patterns associated with the different experimental conditions. Said otherwise, this demonstrates that the input patterns contain information about the cognitive processes recruited when this subject performs the different tasks that have been decoded. The decoding accuracy can then be used as an estimate of the *amount* of available information – the higher accuracy, the more distinguishable the patterns, the larger the amount of information.

The group-level extension of this procedure consists in evaluating whether such information is present throughout the population being studied. For this, a second level statistical analysis is conducted, for instance to test whether the average classification accuracy (or any other relevant summary statistic measured at the single-subject level), computed over the group of participants, is significantly above chance level. This can be done using a variety of approaches (see 2.6 for references). This hierarchical scheme is the one that is most commonly used in the literature. We denote it as Group-MVPA (G-MVPA) in the rest of the present paper and illustrate it on Figure 1.

2.2. Inter-Subject Pattern Analysis (ISPA)

Besides the hierarchical G-MVPA solution, another classifier-based framework exists to evaluate multivariate effects at the group level. Considering the data from all available individuals, one can train a classifier on data from a set of subjects – the training subjects – and evaluate its generalization capability on data from the others – the test subjects. One can then use a cross-validation scheme that shuffles the subjects between the training and test sets, such as leave-one-subject-out or leave-n-subjects-out. In this setting, obtaining an average classification accuracy – this time across folds of the cross-validation – significantly above chance level means that a multivariate effect has been identified and that it is consistent across individuals. We denote this strategy as Inter-Subject Pattern Analysis (ISPA).

In this study, we use a leave-one-subject-out cross-validation in which the model accuracy is repeatedly computed on the data from the left-out subject. Even if other schemes might be preferable to multiply the number of measurements [34], this choice was made to facilitate the comparison of the results obtained with ISPA and G-MVPA, as illustrated on Figure 1.

2.3. Artificial data

The first type of data we use to compare G-MVPA and ISPA is created artificially. We generate a large number of datasets in order to conduct numerous experiments and obtain robust results. Each dataset is composed of 21 subjects (for ISPA: 20 for training, 1 for testing), with data points in two classes labeled as $\mathcal{Y} = \{+1, -1\}$, simulating a paradigm with two experimental conditions. For a given dataset, each subject $s \in \{1, 2, ..., 21\}$ provides 200 labeled observations, 100 per class. We denote the i-th observation and corresponding class label (x_i^s, y_i^s), where $x_i^s \in \mathbb{R}^2$ and $y_i^s \in \mathcal{Y}$. The pattern x_i^s is created as

$$x_i^s = \begin{pmatrix} \cos\theta^s & -\sin\theta^s \\ \sin\theta^s & \cos\theta^s \end{pmatrix} \tilde{x}_i^s,$$

where

- $\tilde{x}_i^s$ is randomly drawn from a 2D Gaussian distribution, $\mathcal{N}(C^+, \Sigma)$ and $\mathcal{N}(C^-, \Sigma)$ if $y_i^s = +1$ or $y_i^s = -1$, respectively, which are defined by their centers $C^+ = (+\frac{d}{2}, 0)$ and $C^- = (-\frac{d}{2}, 0)$, where $d \in \mathbb{R}^+$ and their covariance matrix Σ, here fixed to $\begin{pmatrix} 1 & 0 \\ 0 & 5 \end{pmatrix}$ (see Supplementary Materials for results with other values of Σ);
- θ^s defines a rotation around the origin that is applied to all patterns of subject s; the value of θ^s is randomly drawn from the Gaussian distribution $\mathcal{N}(0, \Theta)$, where Θ defines the within-population variance.

Let $X^s = (x_i^s)_{i=1}^{200}$ and $Y^s = (y_i^s)_{i=1}^{200}$ be the set of patterns and labels for subject s. A full dataset D is defined by

$$D = \bigcup_{s=1}^{s=21} \{X^s, Y^s\}.$$

The characteristics of such a dataset are in fact governed by two parameters:

- d, which defines the distance between the point clouds of each of the two classes, i.e. the multivariate effect size;
- Θ, which controls the amplitude of the rotation that can be applied to the data, separately for each subject: when Θ is small, all the θ^s angles remain small, which means that the data of all subjects are similar; when Θ increases, the differences between subjects become larger; therefore, Θ quantifies the amount of inter-individual variability that exists within the group of 21 subjects for a given dataset.

Figures 2a and 2b illustrate the influence of each of these two parameters. Figure 2c shows different datasets generated with the same values of d and Θ.

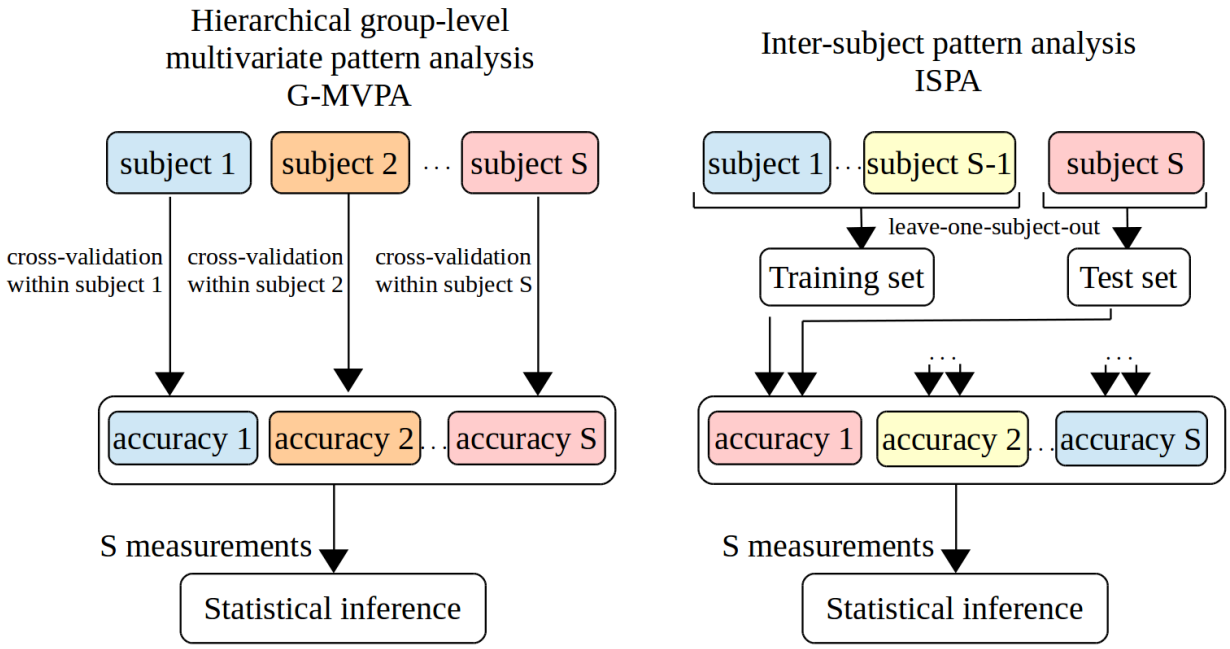

Figure 1: Illustration of the two approaches available to perform classifier-based group-level multivariate analysis. Left: hierarchical group-MVPA (G-MVPA). Right: inter-subject pattern analysis (ISPA). Note that if a leave-one-subject-out cross validation is used for ISPA (as illustrated), the two approaches yield the same number of measurements (equal to the number of subjects S), which allows for an unbiased comparison using the same statistical inference method.

In our experiments we used 13 values for d and 11 values for Θ, $d \in \{0.1, 0.12, 0.14, 0.16, 0.18, 0.2, 0.22, 0.24, 0.26, 0.28, 0.3, 0.4, 0.6\}$, $\Theta \in \{0.2\pi, 0.25\pi, 0.3\pi, 0.35\pi, 0.4\pi, 0.45\pi, 0.5\pi, 0.55\pi, 0.6\pi, 0.65\pi, 0.7\pi\}$, which gives 143 points in the two dimensional parameter space spanned by d and Θ. Note that by changing the value of Θ while keeping Σ constant, we control the relative amounts of within- and between-subject variance, which have been shown to be critical in group-level decoding situations [24]. For each pair (d, Θ), we generated 100 datasets. This yields 14300 datasets, each comprising 21 subjects and a total of 4200 data points. The code for generating these datasets (as well as performing the experiments detailed hereafter) is available online at the following URL: `http://www.github.com/SylvainTakerkart/inter_subject_pattern_analysis`.

2.4. *fMRI data*

We also used two real fMRI datasets that were acquired at the *Centre IRM-INT* in Marseille, France. For both experiments, participants provided written informed consent in agreement with the local guidelines of the South Mediterranean ethics committee.

In the first experiment (hereafter *Dataset1*), fifteen subjects participated in an investigation of the neural basis of cognitive control in the frontal lobe, largely reproducing the experimental procedure described in [21]. Participants lying supine in the MRI scanner were presented with audiovisual stimuli that required a button response, with the right or left thumb. Four inter-stimulus intervals were used equally in a fully randomized order (1.8, 3.5, 5.5, 7.1 seconds), with an average of 4.5 seconds over a session. Data was collected with a 3T Bruker Medspec 30/80 Avance scanner running ParaVision 3.0.2. Eight MRI acquisitions were performed. First, a field map using a double echo Flash sequence recorded distortions in the magnetic field. Six sessions with 60 trials each were recorded, each comprising 133 volumes (EPI sequence, isotropic resolution of $3 \times 3 \times 3$ mm, TE of 30 ms, flip angle of 81.6°, field of view of 192×192 mm, 36 interleaved ascending axial slices acquired within the TR of 2400 ms) encompassing the whole brain parallel to the AC-PC plane. Finally, we acquired a high-resolution T1-weighted anatomical image of each participant (MPRAGE sequence, isotropic voxels of $1 \times 1 \times 1$ mm, field of view of $256 \times 256 \times 180$ mm, $TR = 9.4$ ms, $TE = 4.424$ ms).

In the second experiment (*Dataset2*), thirty-nine subjects were scanned using a *voice localizer* paradigm, adapted from the one analyzed in [29]. While in the scanner, the participants were asked to close their eyes while passively listening to a set of 144 audio stimuli, half of them being voice sounds, the other half being non-vocal. Most of the stimuli were taken from a database created for a previous study [6], while the others were extracted from copyright-free online databases. The paradigm was event-related, with inter-stimulus intervals randomly chosen between 4 and 5 seconds. The images were acquired on a 3T Prisma MRI scanner (Siemens, Eerlangen, Germany) with a 64-channels head coil. A pair of phase-reversed spin echo images was first acquired to estimate a map of the magnetic field. Then, a multi-band gradient echo-planar imaging (EPI)

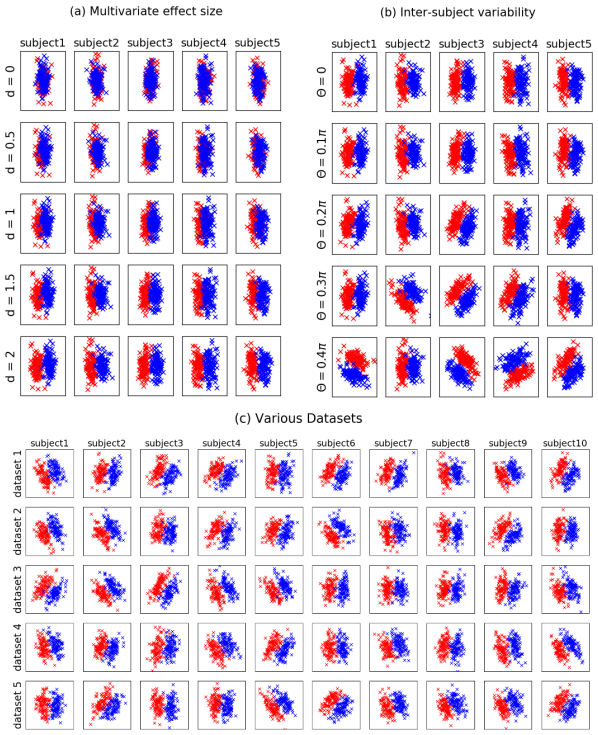

Figure 2: Illustration of the artificial datasets generated with the model described in 2.3. Each line is a subpart of a single dataset (5 subjects shown amongst 21 in (a) and (b), 10 subjects shown in (c)). The data points belonging to the class $y = +1$ and $y = -1$ are shown in blue and red, respectively. (a): influence of the d parameter (increasing effect size from top to bottom). (b): influence of the Θ parameter (increasing inter-individual variability from top to bottom). (c) five datasets obtained with the same values of the two parameters ($d = 2$ and $\Theta = 0.2\pi$).

sequence with a factor of 5 was used to cover the whole brain and cerebellum with 60 slices during the TR of 955 ms, with an isotropic resolution of $2 \times 2 \times 2$ mm, a TE of 35.2 ms, a flip angle of 56 degrees and a field of view of 200×200 mm for each slice. A total of 792 volumes were acquired in a single run of 12 minutes and 36 seconds. Then, a high resolution 3D T1 image was acquired for each subject (isotropic voxel size 0.8 mm^3, $TR = 2400$ ms, $TE = 2.28$ ms, field of view of $256 \times 256 \times 204.8$ mm). *Dataset2* is part of the InterTVA data set [1], which is fully available online [1].

2.5. *fMRI data analysis*

The two datasets were processed using the same sets of operations. The pre-processing steps were performed in SPM12[2]. They included co-registration of the EPIs with the T1 anatomical image, correction of the image distortions using the field maps, motion correction of the EPIs, construction of a population-specific anatomical template using the DARTEL method, transformation of the DARTEL template into MNI space and warping of the EPIs into this template space. Then, a general linear model was set up with one regressor per trial, as well as other regressors of non interest such as motion parameters, following the least-squares-all approach described in [26]. The estimation of the parameters of this model yielded a set of beta maps that was each associated with a given experimental trial. The beta values contained in these maps allowed constructing the vectors that serve as inputs to the decoding algorithms, that therefore operate on single trials. We obtained 360 and 144 beta maps per subject for *Dataset1* and *Dataset2* respectively. No spatial smoothing was applied on these data for the results presented below (the results obtained with smoothing are provided as Supplementary Materials).

For these real fMRI datasets, we performed a searchlight decoding analysis [23], which allows to map local multivariate effects by sliding a spherical window throughout the whole brain and performing independent decoding analyses within each sphere. For our experiments, we exploited the searchlight implementation available in nilearn[3] to allow obtaining the single-fold accuracy maps necessary to perform inference. For *Dataset1*, the decoding task was to guess whether the participant had used his left vs. right thumb to answer during the trial corresponding to the activation pattern provided to classifier. For G-MVPA, the within-subject cross-validation followed a leave-two-sessions-out scheme. For *Dataset2*, the binary classification task consisted in deciphering whether the sound presented to the participant was vocal or non-vocal. For G-MVPA, because a single session was available, we used an 8-fold cross-validation. Finally, all experiments were repeated with five different values of the searchlight radius ($r \in \{4$ mm, 6 mm, 8 mm, 10 mm, 12 mm$\}$).

2.6. *Classifiers, Statistical inference and performance evaluation*

In practice, we employed the logistic regression classification algorithm (with l_2 regularization and a regularization weight of $C = 0.1$), as available in the scikit-learn[4] python module, for both artificial and real fMRI data. The logistic regression has been widely used in neuroimaging because it is a linear model that enables neuroscientific interpretation by examining the weights of the model, and because it provides results on par with state of the art methods while offering an appealing computational efficiency [30].

In order to perform statistical inference at the group level, the common practice is to use a t-test on the decoding accuracies. Such a test assesses whether the null hypothesis of a chance-level average accuracy can be rejected, which would reveal the existence of a multivariate difference between conditions at the group level (note that, as detailed in 2.1 and 2.2, the rejection of this null hypothesis provides different insights on

[1] https://openneuro.org/datasets/ds001771
[2] https://www.fil.ion.ucl.ac.uk/spm/
[3] http://nilearn.github.io/
[4] https://scikit-learn.org/stable/

the group-level effect depending on whether G-MVPA or ISPA is used).

However, several criticisms have been raised in the literature against this approach, namely on the nature of the statistical distribution of classification accuracies [28, 2], on the non-directional nature of the identified group-information [13] or on the fact that the results can be biased by confounds [33]. This has led to the development of alternative methods (see e.g. [28, 5, 31, 9, 2]), all dedicated to G-MVPA.

Because our objective is to compare the results given by G-MVPA and ISPA in a fair manner, i.e using the same statistical test, we used a permutation test [27] which allows overcoming some of the aforementioned limitations. This test assesses the significance of the average accuracy at the group-level in a non-parametric manner for all the experiments conducted in the present study, whether conducted with G-MVPA or ISPA. Furthermore, this choice allowed maintaining the computational cost at a reasonable level, a condition that other alternatives, e.g inspired by [31], would not have met (see the Supplementary Materials for a longer discussion on this matter). In practice, for the real fMRI experiments, we used the implementation offered in the SnPM toolbox[5] to analyse the within-subject (for G-MVPA) or the single-fold (for the inter-subject cross-validation of ISPA) accuracy maps, with 1000 permutations and a significance threshold ($p < 0.05$, FWE corrected). For the simulations that used the artificial datasets, we used an in-house implementation of the equivalent permutation test (also available in our open source code; see 2.3), with 1000 permutations and a threshold at $p < 0.05$. Critically, it should be noted that the same number of samples were available for this statistical procedure when using G-MVPA or ISPA, as shown on Figure 1.

In order to compare the group-level decoding results provided by G-MVPA and ISPA, we use the following set of metrics. For the artificial data, we generated 100 datasets at each of the 143 points of the two dimensional parameter space spanned by the two parameters d and Θ. For each of these datasets, we estimate the probability p to reject the null hypothesis of no group-level decoding. We then simply count the number of datasets for which this null hypothesis can be rejected, using the $p < 0.05$ threshold, which we denote N_G and N_I for G-MVPA and ISPA, respectively. For the two real fMRI datasets, we examine the thresholded statistical map obtained for each experiment. We then compare the maps obtained by G-MVPA and ISPA by computing the size and maximum statistic of each cluster, as well as quantitatively assessing their extent and localization by measuring how they overlap.

3. Results

In this section, we present the results obtained when comparing G-MVPA and ISPA on both artificial and real fMRI datasets. With the artificial datasets, because we know the ground truth, we can unambiguously quantify the differences between the two strategies. Our focus is therefore on the characterization of the space spanned by the two parameters that control the characteristics of the data to evaluate which of these two strategies provides better detection power. For the real datasets, we do not have access to a ground truth. After having assessed the consistency of the obtained results with previously published work, we therefore focus on describing the differences between the statistical maps produced by G-MVPA and ISPA, examine the influence of the searchlight radius, and try to relate these results to the ones obtained on the artificial datasets.

3.1. Results for artificial datasets

The results of the application of G-MVPA and ISPA on the 14300 datasets that were artificially created are summarized in Tables 1, 2 and 3. In order to facilitate grasping the results on this very large number of datasets, we proceed in two steps.

First, we represent the two-dimensional parameter space spanned by d and Θ as a table where the columns and lines represent a given value for these two parameters, respectively. The values in these tables are the number of datasets N_G and N_I (out of the 100 datasets available for each cell) for which a significant group level decoding accuracy ($p < 0.05$, permutation test) is obtained with G-MVPA (Table 1) or ISPA (Table 2). In order to analyse these two tables, we performed a multiple linear regression where d and Θ are the independent variables used to explain the number of significant results in each cell. In Table 1, the effect of d is significant ($F_d^{G-WSPA} = 941.75$, $p_d^{G-WSPA} < 10^{-10}$), but the effect of Θ is not ($F_\Theta^{G-WSPA} = 0.83$, $p_\Theta^{G-SPA} = 0.36$), while in Table 2, both factors have significant effects ($F_d^{ISPA} = 135.20$, $p_d^{ISPA} < 10^{-10}$; $F_\Theta^{ISPA} = 774.27$, $p_\Theta^{ISPA} < 10^{-10}$). This means that, as expected, the effect size d has an effect on the detection power of both G-MVPA and ISPA, i.e the smaller the effect size, the more difficult the detection. But the amount of inter-individual variability, here quantified by Θ, influences the detection capability of ISPA, but not the one of G-MVPA. This produces the rectangle-like area visible in green on Table 1 and the triangle-like area visible in red on Table 2. When the inter-individual variability is low, ISPA can detect significant effects even with very small effect sizes. When the variability increases, the detection power of ISPA decreases – i.e. for a given effect size, the number of datasets for which ISPA yields a significant result decreases, but the one of G-MVPA remains constant.

Secondly, in order to easily depict the compared behaviors of G-MVPA and ISPA, we *overlapped* the results of the two strategies into Table 3. In this third table, the blue cells indicate that $N_G \geqslant 50$ and $N_I \geqslant 50$ (i.e. that both G-MVPA and ISPA produce significant results in more than half of the 100 datasets), while the green and red regions contain cells where it is the case only for G-MVPA or ISPA respectively (i.e. $N_G \geqslant 50$ and $N_I < 50$ in green cells; $N_I \geqslant 50$ and $N_G < 50$ in red cells). Note that for completeness, we also used different values of this arbitrary threshold set at 50, which did not qualitatively change the nature of the results described below (hence these results are not shown). We observe a large blue region in which both strategies provide concordant detections, for the largest values of the effect size d and with

[5] `http://warwick.ac.uk/snpm`

Table 1: Number of datasets N_G (out of 100) for which G-MVPA provides significant group decoding (in green: cells where $N_G \geq 50$)

variability \ effect size	0.1	0.12	0.14	0.16	0.18	0.2	0.22	0.24	0.26	0.28	0.3	0.4	0.6
0.7π	7	11	15	22	27	36	40	44	53	59	68	96	100
0.65π	9	14	16	23	29	36	39	45	55	63	70	98	100
0.6π	13	16	17	25	27	35	44	53	58	71	76	95	100
0.55π	10	14	17	21	25	32	37	46	50	61	76	96	100
0.5π	7	8	15	17	22	30	36	46	55	59	64	94	100
0.45π	4	7	13	14	22	32	39	46	51	62	69	96	100
0.4π	8	11	18	22	26	31	40	49	54	63	72	97	100
0.35π	4	7	15	24	34	37	46	51	61	61	68	96	100
0.3π	10	14	24	26	31	40	46	57	58	71	78	95	100
0.25π	9	13	20	25	32	43	45	53	60	62	69	94	100
0.2π	9	12	15	19	28	34	39	50	59	67	75	95	100

Table 2: Number of datasets N_I (out of 100) for which ISPA provides significant group decoding (in red: cells where $N_I \geq 50$)

variability \ effect size	0.1	0.12	0.14	0.16	0.18	0.2	0.22	0.24	0.26	0.28	0.3	0.4	0.6
0.7π	8	8	9	10	11	10	10	10	8	10	10	9	13
0.65π	5	8	8	8	9	10	9	10	14	14	14	13	19
0.6π	8	13	12	13	15	15	14	17	16	18	20	20	21
0.55π	13	13	14	15	20	19	23	22	25	26	26	25	27
0.5π	16	15	16	22	24	24	28	27	29	29	30	38	45
0.45π	19	21	22	26	29	32	34	42	47	53	53	59	67
0.4π	22	28	33	34	39	41	42	49	49	50	54	69	85
0.35π	21	27	32	37	44	50	55	61	68	69	74	85	93
0.3π	25	30	39	46	60	67	70	74	82	83	90	98	99
0.25π	44	56	63	69	73	79	84	90	94	96	96	100	100
0.2π	42	55	63	71	80	86	91	93	94	98	98	100	100

Table 3: Visual comparison of G-MVPA vs. ISPA (in blue: cells where both $N_G \geq 50$ and $N_I \geq 50$; in green: cells where $N_G \geq 50$ and $N_I < 50$; in red: cells where $N_G < 50$ and $N_I \geq 50$).

variability \ effect size	0.1	0.12	0.14	0.16	0.18	0.2	0.22	0.24	0.26	0.28	0.3	0.4	0.6
0.7π													
0.65π													
0.6π													
0.55π													
0.5π													
0.45π													
0.4π													
0.35π													
0.3π													
0.25π													
0.2π													

a moderately low amount of inter-individual variability. Interestingly, the green and red regions, where one strategy detects a group-level effect while the other does not, also take an important area in the portion of the parameter space that was browsed by our experiments, which means that the two strategies can disagree. G-MVPA can provide a positive detection when the inter-individual variability is very large, while ISPA cannot (green region). But ISPA is the only strategy that offers a positive detection for very small effect sizes, requiring a moderate inter-individual variability (red region).

3.2. Results for fMRI datasets

3.2.1. Qualitative observations

For our two real datasets, the literature provides clear expectations about brain areas involved in the tasks performed by the participants and the associated decoding question addressed in our experiments. The active finger movements performed by the participants during the acquisition of *Dataset1* are known to recruit contralateral primary motor and sensory as well as secondary sensory cortices, ipsilateral dorsal cerebellum as well as the medial supplementary motor area [25]. In *Dataset2*, the participants were passively listening to vocal and non-vocal sounds. The contrast, or decoding, of these two types of stimuli is classically used to detect the so-called temporal voice areas, which are located along the superior temporal cortex (see e.g. [29]). We now describe the results obtained with G-MVPA and ISPA with respect to this priori knowledge.

The searchlight decoding analyses performed at the group level were all able to detect clusters of voxels where the decoding performance was significantly above chance level ($p < 0.05$, FWE-corrected using permutation tests) with both G-MVPA and ISPA, for *Dataset1* and *Dataset2* and with all sizes of the spherical searchlight. The detected clusters were overall consistent across values of the searchlight radius, with an increasing size of each cluster when the radius increases. In *Dataset1*,

both strategies uncovered two large significant clusters located symmetrically in the left and right motor cortex. Additionally, ISPA was able to detect other significant regions located bilaterally in the dorsal part of the cerebellum and the parietal operculum, as well as a medial cluster in the supplementary motor area (note that some of these smaller clusters also become significant with G-MVPA with the larger searchlight radii). These areas were indeed expected to be involved bilaterally given that button presses were given with both hands in this experiment. In *Dataset2*, both G-MVPA and ISPA yielded two large significant clusters in the temporal lobe in the left and right hemispheres, which include the primary auditory cortex as well as higher level auditory regions located along the superior temporal cortices, matching the known locations of the temporal voice areas. Figure 3 provides a representative illustration of these results, for a radius of 6 mm.

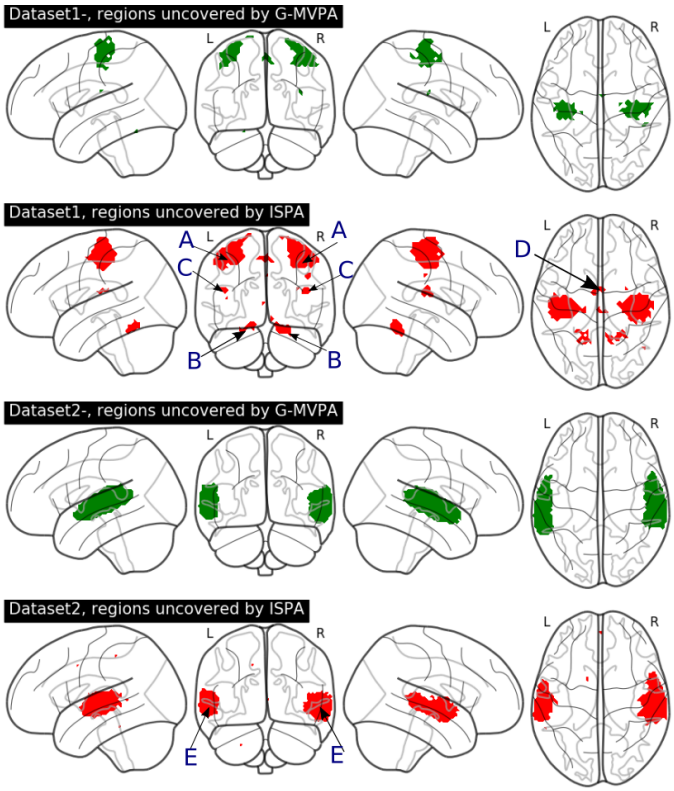

Figure 3: Illustration of the results of the group-level searchlight decoding analysis for a 6 mm radius. Top two rows: *Dataset1*; bottom two rows: *Dataset2*. Brain regions found significant using G-MVPA and ISPA are depicted in green and red, respectively. A: primary motor and sensory cortices B:ipsilateral dorsal cerebellum C: medial supplementary motor area D: secondary sensory cortices E: superior temporal cortex

3.2.2. Quantitative evaluation

Our quantitative evaluation focuses on the two largest clusters uncovered in each dataset, i.e. the ones in the motor cortex for *Dataset1* and the ones in the temporal lobe for *Dataset2*. We first examine the size of these clusters, separately for each hemisphere and each of the five values of the searchlight radius. The results are displayed in the left column of Figure 4. In almost all cases, the size of the significant clusters increased with the searchlight radius (left column). Moreover, the cluster located in the right hemisphere is consistently larger than the one on the left. In *Dataset1*, the cluster detected by ISPA is larger than the one detected by G-MVPA, regardless of the hemisphere, while in *Dataset2*, it is G-MVPA that yields larger clusters (except for a 4 mm radius where the sizes are similar). Then, we study the peak value of the t statistic obtained in each cluster (right column of Figure 4). In *Dataset1*, the peak t value is higher for ISPA than G-MVPA, for all values of the radius. In *Dataset2*, ISPA yields higher peak t values than G-MVPA for the searchlight radii smaller or equal than 8 mm, and lower peak t values for the larger radius values.

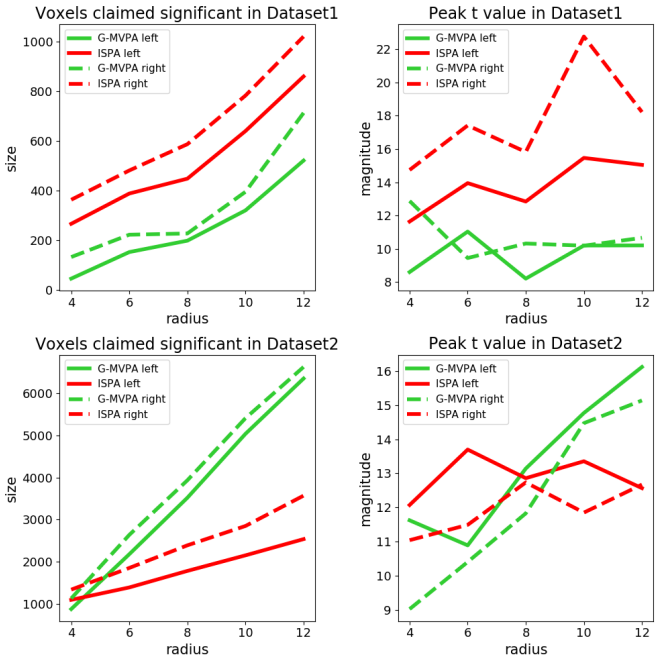

Figure 4: Quantitative evaluation of the results obtained on the real fMRI datasets for G-MVPA (green curves) and ISPA (red curves). Solid and dashed lines for the largest cluster in the left and right hemispheres respectively. Left column: size of the significant clusters. Right column: peak t statistic. Top vs. bottom row: results for *Dataset1* and *Dataset2* respectively.

Then, we quantify the amount of overlap between the clusters found by G-MVPA and ISPA, by splitting the voxels into three sub-regions: voxels uncovered only by ISPA, only by G-MVPA or by both strategies (overlap). Figure 5 provides an illustration of these sub-regions, which shows that the overlap region (in blue) is located at the core of the detected clusters, while the voxels significant for only one strategy are located in the periphery; these peripheral voxels appear to be mostly detected by ISPA for *Dataset1* (red voxels) and by G-MVPA for *Dataset2* (green voxels). Figure 6 shows the voxel counts in

each sub-region, which confirms this visual inspection. Overall, the size of the sub-region found by the two strategies increases with the searchlight radius. The ISPA-only sub-region is larger in *Dataset1* than in *Dataset2*, representing between 38% and 83% of all significant voxels. Conversely in *Dataset2*, the G-MVPA-only sub-region is more important – with a percentage of all significant voxels comprised between 18% and 60%.

We also count the number of voxels in each sub-region for each hemisphere. Figure 6 shows that for both datasets, the clusters in the right hemisphere are larger than in the left hemisphere. For both hemispheres, in most cases the number of voxels in each sub-region increases as the searchlight radius increases. However, in *Dataset1*, the number of voxels found only by G-MVPA is much smaller than that of overlap and ISPA-only sub-regions with all five radius values. In contrast, in *Dataset2* the number of voxels in ISPA-only sub-regions decreases for the four smallest values of the searchlight radius, and voxels only uncovered by ISPA are much fewer than those found only by G-MVPA.

4. Discussion

4.1. G-MVPA and ISPA provide different results

In this study, we have performed experiments on both real and artificial functional neuroimaging data in order to compare two group-level MVPA schemes that rely on classifier-based decoding analyses: the vastly used G-MVPA, and ISPA. Our results show that both strategies can offer equivalent results in some cases, i.e. that they both detect significant group-level multivariate effects in similar regions of the cortex for our two real fMRI datasets, and in parts of the two-dimensional parameter space browsed using our artificially generated datasets, but that their outcomes can also differ significantly. For instance, in *Dataset1*, ISPA was the only strategy that detected multivariate group-level effects in several regions such as the supplementary motor area, the bilateral parietal operculum and dorsal cerebellum, for most of the searchlight radii that we tested (see an example on Figure 3 with a 6 mm radius). Furthermore, when a region is detected by both strategies, it usually differs in its size, extent and/or precise location, resulting in partial overlap; in most cases, the areas of concordance between the two strategies appeared to be centrally located, while the disagreements are located towards the periphery: in some areas, G-MVPA detects a group-level effect while ISPA does not, and inversely in other areas. Note that for *Dataset2*, our results generalize some of the observations reported in [13] with a different, yet comparable, framework of analysis, on a closely related data set.

Surprisingly, the peripheral behaviors were not consistent across the two real fMRI datasets: on *Dataset1*, ISPA only was able to detect effects on the periphery of the core region where both strategies were equally effective, while on *Dataset2*, it was G-MVPA which provided significant results on the periphery. The results of the experiments conducted on the artificial datasets can actually shed some light on these results, thanks to the clear dissociation that was observed in the two-dimensional parameter space browsed to control the properties of the data. Indeed, ISPA is the only strategy that allows detecting smaller multivariate effects when the inter-individual variability remains moderate, which is the case in the largest regions detected in *Dataset1* because they are located in the primary motor cortex, the *primary* nature of this region limiting the amount of inter-subject variability. On the opposite, the peripheral parts of the temporal region detected in *Dataset2* are located anteriorly and posteriorly to the primary auditory cortex, towards higher-level auditory areas where the inter-individual variability is higher, a situation in which G-MVPA revealed more effective in the experiments conducted with our artificial data.

4.2. ISPA: larger training sets improve detection power

Our experiments revealed a very important feature offered by the ISPA strategy: its ability to detect smaller multivariate effects. On the one hand, this greater detection power was explicitly demonstrated through the simulations performed on artificial data, where the multivariate effect size was one of the two parameters that governed the generation of the data; we showed that with an equal amount of inter-individual variability, ISPA was able to detect effects as small as half of what can be detected by G-MVPA. Furthermore, on both real fMRI datasets, ISPA was able to detect significant voxels that were not detected using G-MVPA, in a large amount in *Dataset1*, and to a lesser extent in *Dataset2*. This detection power advantage is of great importance, since detecting weak distributed effects was one of the original motivations for the use of MVPA [15].

This greater detection power of ISPA is in fact the result of the larger size of the training set available: indeed, when the number of training examples is small, the performance of a model overall increases with the size of the training set, until an asymptote that is reached with large training sets – as encountered in computer vision problems where millions of images are available from e.g. ImageNet[6]. In the case of functional neuroimaging where an observation usually corresponds to an experimental trial, we usually have a few dozen to a few hundred samples per subject, which clearly belongs to the *small sample size* regime, i.e. very far from the asymptote. In this context, ISPA offers the advantage to multiply the number of training samples by a factor equal to the number of subjects in the training set, which is of great value. However, here, the increased sample size comes at the price of a larger heterogeneity in the training set, because of the differences that can exist between data points recorded in different subjects. If these differences are too large, they can represent an obstacle for learning, but if more moderate, the inter-subject variability can reveal beneficial by increasing the diversity of the training set. The fact that we observe a higher detection power with ISPA than with G-MVPA suggests that we are in the latter situation.

4.3. ISPA offers straightforward interpretation

When using the ISPA strategy, obtaining a positive result means that the model has learnt an implicit rule from the training data that provides statistically significant generalization power

[6] `http://www.image-net.org`

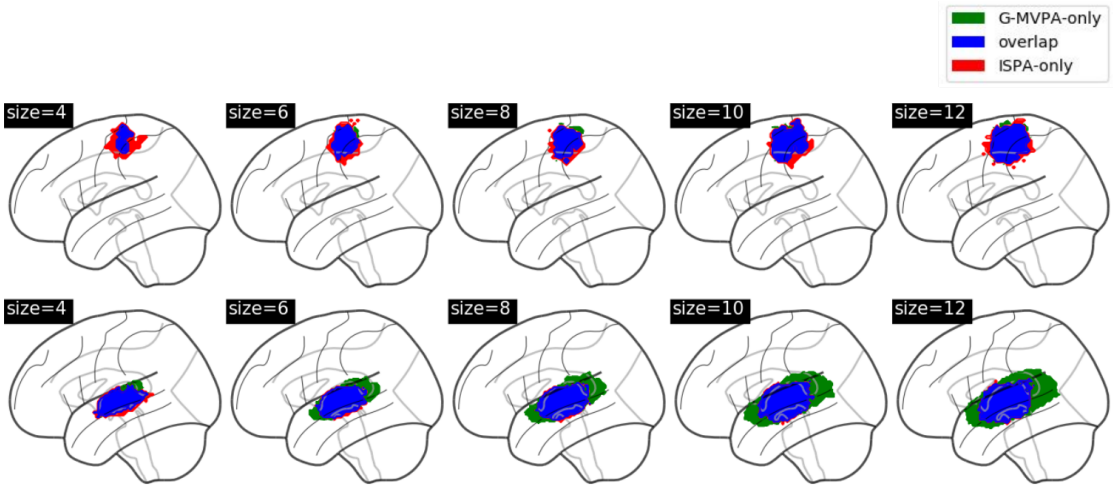

Figure 5: Comparison of the clusters detected by G-MVPA and ISPA for the different values of the searchlight radius, in *Dataset1* (top row) and *Dataset2* (bottom row).

on data from new subjects. Since a cross-validation of the type leave-one-subject-out or leave-n-subjects-out is performed on the available data to quantitatively assess such results, it allows to draw inference on the full population from which the group of participants was drawn, including individuals for which no data was available. As previously pointed out in [22], the interpretation that follows is straightforward: a significant effect detected with ISPA implies that some information has been identified to be consistent throughout the full population. In more details, this means that the modulations of the multivariate patterns according to the experimental conditions that were the object of the decoding analysis are consistent throughout the population, at least at the resolution offered by the modality used for the acquisition. This is the case for all voxels colored blue and red on Figure 5.

4.4. G-MVPA is more sensitive to idiosyncrasies

A significant result detected by G-MVPA but not ISPA – i.e. the green voxels on Figure 5, indicates that there is information at the population level in the input patterns that can discriminate the different experimental conditions, but that the nature of the discriminant information present in the input voxels differs across individuals. In other words, G-MVPA has detected idiosyncratic pattern modulations between conditions, which can be of great neuroscientific interest (see e.g. [7]), that could not have been identified with ISPA. This could be caused by two phenomenons. First, it could mean that the underlying coding strategy is nonetheless invariant across individuals, but that the nature of the data or of the feature space used in this analysis does not allow to identify it as such, e.g. because of an unperfect inter-subject registration of the functional maps. One would then need to acquire additional data using a different modality ([8]) or to transform the feature space (e.g. using methods such as [14], [32] or [11]) in order to attempt to make this invariance explicit. Secondly, it could also mean that the neural code is simply intrinsically different across subjects, for instance because several strategies had been employed by different individuals to achieve the same task, or because each subject employs its own idiosyncratic neural code. G-MVPA therefore only provides part of the answer, which makes the interpretation much less direct.

Note that beyond searchlight analyses, this potential ambiguity could also occur with decoding performed in pre-defined regions of interest. Although such ROI-based decoding are vastly analysed at the group level using G-MVPA, numerous papers interpret the results as if G-MVPA allows identifying population-wise common coding principles, which cannot be claimed with only G-MVPA. These limitations have been pointed out previously in the literature, as in e.g. [33], [2] or [13], and we feel that the community should tackle this question more firmly. This could start by defining what a group-level multivariate analysis should seek – a consistent *amount* or *nature* of the information. Finally, because G-MVPA and ISPA are somehow complementary, one could think about using both types of analysis to better assess neural coding principles.

4.5. A computational perspective

Finally, we examine here some practical considerations that are important for the practitioner, by comparing the computational cost of G-MVPA and ISPA, and the availability of ready-to-use software implementations.

To assess the computational complexity of the two approaches, we first compare the number of classifiers that need to be trained for a full group analysis. Using G-MVPA, we need to train K classifiers per subject, where K is the chosen number of within-subject cross-validation folds, so KS classifiers in total (where S is the number of available subjects). For ISPA, the number of cross-validation folds equals to S (for leave-one-subject-out), meaning we need to train a total of S classifiers. The training time of a classifier also depends on the number of training examples: it is linear for classifiers such as logistic regression (when using gradient-based optimizers [3]), and

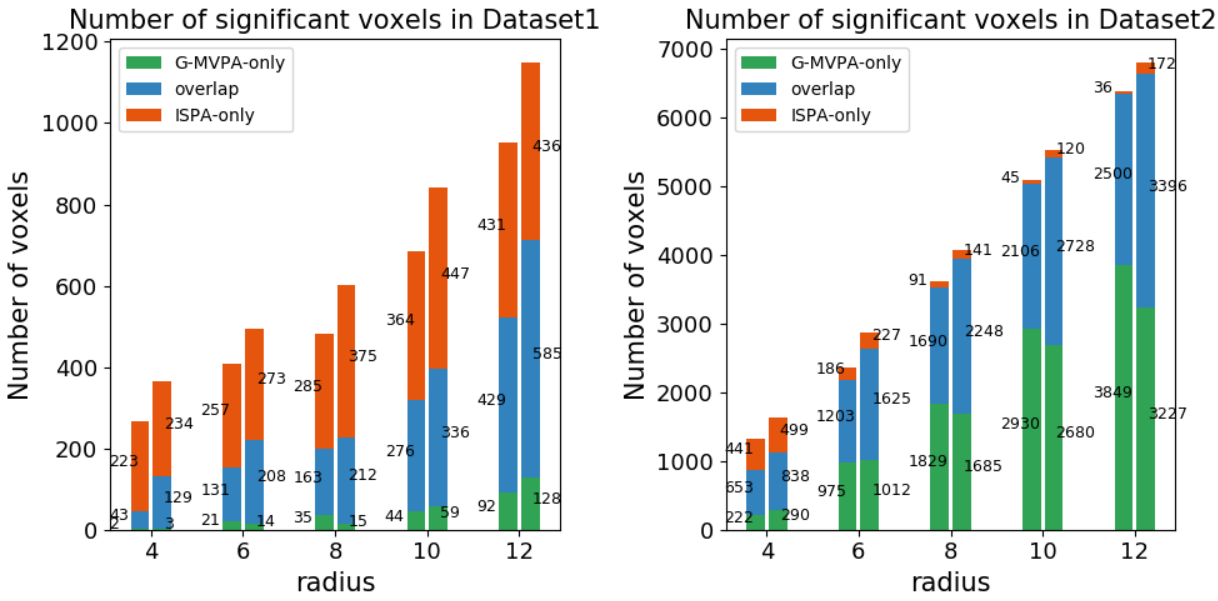

Figure 6: Comparison of the voxel counts detected by G-MVPA-only (green), ISPA-only (red) or both (blue) for the different values of the searchlight radius, in *Dataset1* (left) and *Dataset2* (right).

quadratic for e.g. support vector machines [4]. Assuming we have n examples per subject, the number of training examples available for each classifier is $\frac{(K-1)n}{K}$ for G-MVPA and $(S-1)n$ for ISPA. Overall, with linear-time classifiers, the total complexity of a group-level decoding analysis amounts to $O(nKS)$ for G-MVPA and $O(nS^2)$ for ISPA, which makes them almost equivalent if one assumes that K and S are of the same order of magnitude. With quadratic-time classifiers, the total complexity is $O(n^2KS)$ for G-MVPA and $O(n^2S^3)$ for ISPA, which makes ISPA significantly more costly. We therefore advice to use linear-time classifiers such as logistic regression to perform ISPA analyses, particularly with searchlight decoding where the computational cost is further multiplied by the number of voxels. Furthermore, note that thanks to its hierarchical nature, G-MVPA can be performed in an incremental manner for a low computational cost as participants get scanned: every time data from a new subject becomes available during the acquisition campaign, it suffices to run within-subject decoding for this new subject, which costs $O(nK)$, plus the statistical test. This offers more flexibility for the experimenter than with the inter-subject scheme, for which performing IPSA every time a new subject is scanned amounts to re-doing a full analysis on all the subjects.

In terms of software implementation, because within-subject analyses have been the standard since the advent of MVPA, all software packages provide well documented examples for such analyses which are the base tool for G-MVPA. Even if it is not the case for ISPA, it is easy to obtain an equivalent implementation because to perform inter-subject decoding, one simply need to i) have access to the data from all subjects, and ii) set up a leave-one-subject-out cross-validation, these two operations being available in all software packages. As an example, we provide the code to perform ISPA searchlight decoding from pre-processed data available online, which allows reproducing the results described in the present paper on *Dataset2*: `http://www.github.com/SylvainTakerkart/inter_subject_pattern_analysis`.

5. Conclusion

In this paper, we have compared two strategies that allow performing group-level decoding-based multivariate pattern analysis of task-based functional neuroimaging experiments: the first is the standard method that aggregates within-subject decoding results and a second one that directly seeks to decode neural patterns at the group level in an inter-subject scheme. Both strategies revealed effective but they only provide partially concordant results. Inter-subject pattern analysis offers a higher detection power to detect weak distributed effects and facilitate the interpretation while the results provided by the hierarchical approach necessitate further investigation to raise potential ambiguities. Furthermore, because it allows identifying group-wise invariants from functional neuroimaging patterns, inter-subject pattern analysis is a tool of choice to identify neuromarkers [12] or brain signatures [22], making it a versatile scheme for population-wise multivariate analyses.

Acknowledgments

This work was carried out within the Institut Convergence ILCB (ANR-16-CONV-0002). It was granted access to the HPC resources of Aix-Marseille Université financed by the project Equip@Meso (ANR-10-EQPX-29-01) of the French program *Investissements d'Avenir*. The acquisition of the data was made

possible thanks to the infrastructure France Life Imaging (11-INBS-0006) of the French program *Investissements d'Avenir*, as well as specific grants from the *Templeton Foundation* (40463) and the *Agence Nationale de la Recherche* (ANR-15-CE23-0026).

References

[1] Aglieri, V., Cagna, B., Belin, P., Takerkart, S., 2019. InterTVA. A multimodal MRI dataset for the study of inter-individual differences in voice perception and identification. OpenNeuro URL: https://openneuro.org/datasets/ds001771.

[2] Allefeld, C., Grgen, K., Haynes, J.D., 2016. Valid population inference for information-based imaging: From the second-level t -test to prevalence inference. NeuroImage 141, 378–392. doi:10.1016/j.neuroimage.2016.07.040.

[3] Bach, F., 2014. Adaptivity of averaged stochastic gradient descent to local strong convexity for logistic regression. The Journal of Machine Learning Research 15, 595–627.

[4] Bottou, L., Lin, C.J., 2007. Support vector machine solvers. Large scale kernel machines 3, 301–320.

[5] Brodersen, K.H., Daunizeau, J., Mathys, C., Chumbley, J.R., Buhmann, J.M., Stephan, K.E., 2013. Variational Bayesian mixed-effects inference for classification studies. NeuroImage 76, 345–361. URL: https://linkinghub.elsevier.com/retrieve/pii/S1053811913002371, doi:10.1016/j.neuroimage.2013.03.008.

[6] Capilla, A., Belin, P., Gross, J., 2012. The Early Spatio-Temporal Correlates and Task Independence of Cerebral Voice Processing Studied with MEG. Cerebral Cortex 23, 1388–1395. doi:10.1093/cercor/bhs119.

[7] Charest, I., Kievit, R.A., Schmitz, T.W., Deca, D., Kriegeskorte, N., 2014. Unique semantic space in the brain of each beholder predicts perceived similarity. Proceedings of the National Academy of Sciences 111, 14565–14570. doi:10.1073/pnas.1402594111.

[8] Dubois, J., de Berker, A.O., Tsao, D.Y., 2015. Single-Unit Recordings in the Macaque Face Patch System Reveal Limit ations of fMRI MVPA. Journal of Neuroscience 35, 2791–2802. doi:10.1523/JNEUROSCI.4037-14.2015.

[9] Etzel, J.A., 2015. MVPA Permutation Schemes: Permutation Testing for the Group Level, in: 2015 International Workshop on Pattern Recognition in NeuroImaging, pp. 65–68. doi:10.1109/PRNI.2015.29.

[10] Etzel, J.A., Valchev, N., Gazzola, V., Keysers, C., 2016. Is brain activity during action observation modulated by the perceived fairness of the actor? PLoS One 11, e0145350.

[11] Fuchigami, T., Shikauchi, Y., Nakae, K., Shikauchi, M., Ogawa, T., Ishii, S., 2018. Zero-shot fMRI decoding with three-dimensional registration based on diffusion tensor imaging. Scientific Reports 8. doi:10.1038/s41598-018-30676-3.

[12] Gabrieli, J., Ghosh, S., Whitfield-Gabrieli, S., 2015. Prediction as a Humanitarian and Pragmatic Contribution from Human Cogniti ve Neuroscience. Neuron 85, 11–26. URL: http://linkinghub.elsevier.com/retrieve/pii/S0896627314009672, doi:10.1016/j.neuron.2014.10.047.

[13] Gilron, R., Rosenblatt, J., Koyejo, O., Poldrack, R.A., Mukamel, R., 2017. What's in a pattern? examining the type of signal multivariate analysis uncovers at the group level. NeuroImage 146, 113–120.

[14] Haxby, J., Guntupalli, J., Connolly, A., Halchenko, Y., Conroy, B., Gobbini, M., Hanke, M., Ra madge, P., 2011. A Common, High-Dimensional Model of the Representational Space in Human Ventral Temporal Cortex. Neuron 72, 404–416. doi:10.1016/j.neuron.2011.08.026.

[15] Haxby, J.V., Connolly, A.C., Guntupalli, J.S., 2014. Decoding Neural Representational Spaces Using Multivariate Pattern Analysis. Annual Review of Neuroscience 37, 435–456. URL: http://dx.doi.org/10.1146/annurev-neuro-062012-170325, doi:10.1146/annurev-neuro-062012-170325.

[16] Haxby, J.V., Gobbini, M.I., Furey, M.L., Ishai, A., Schouten, J.L., Pietrini, P., 2001. Distributed and Overlapping Representations of Faces and Objects in Ventral Temporal Cortex. Science 293, 2425–2430.

[17] Helfinstein, S.M., Schonberg, T., Congdon, E., Karlsgodt, K.H., Mumford, J.A., Sabb, F.W., Cannon, T.D., London, E.D., Bilder, R.M., Poldrack, R.A., 2014. Predicting risky choices from brain activity patterns. Proceedings of the National Academy of Sciences 111, 2470–2475.

[18] Izuma, K., Shibata, K., Matsumoto, K., Adolphs, R., 2017. Neural predictors of evaluative attitudes toward celebrities. Social cognitive and affective neuroscience 12, 382–390.

[19] Jiang, J., Summerfield, C., Egner, T., 2016. Visual Prediction Error Spreads Across Object Features in Human Visual Cortex. The Journal of Neuroscience 36, 12746–12763. doi:10.1523/JNEUROSCI.1546-16.2016.

[20] Kim, J., Wang, J., Wedell, D.H., Shinkareva, S.V., 2016. Identifying core affect in individuals from fmri responses to dynamic naturalistic audiovisual stimuli. PloS one 11, e0161589.

[21] Koechlin, E., Jubault, T., 2006. Broca's Area and the Hierarchical Organization of Human Behavior. Neuron 50, 963–974. URL: https://linkinghub.elsevier.com/retrieve/pii/S0896627306004053, doi:10.1016/j.neuron.2006.05.017.

[22] Kragel, P.A., Koban, L., Barrett, L.F., Wager, T.D., 2018. Representation, Pattern Information, and Brain Signatures: From Neurons to Neuroimaging. Neuron 99, 257–273. URL: https://linkinghub.elsevier.com/retrieve/pii/S089662731830477X, doi:10.1016/j.neuron.2018.06.009.

[23] Kriegeskorte, N., Goebel, R., Bandettini, P., 2006. Information-based functional brain mapping. Proceedings of the National Academy of Sciences 103, 3863–3868.

[24] Lindquist, M.A., Krishnan, A., Lpez-Sol, M., Jepma, M.e., Woo, C.W., Koban, L., Roy, M., Atlas, L.Y., Schmidt, L., Chang, L.J., Reynolds Losin, E.A., Eisenbarth, H., Ashar, Y.K., Delk, E., Wager, T.D., 2017. Group-regularized individual prediction: theory and application to pain. NeuroImage 145, 274–287. doi:10.1016/j.neuroimage.2015.10.074.

[25] Mima, T., Sadato, N., Yazawa, S., Hanakawa, T., Fukuyama, H., Yonekura, Y., Shibasaki, H., 1999. Brain structures related to active and passive finger movements in man. Brain 122, 1989–1997. URL: https://academic.oup.com/brain/article-lookup/doi/10.1093/brain/122.10.1989, doi:10.1093/brain/122.10.1989.

[26] Mumford, J.A., Turner, B.O., Ashby, F.G., Poldrack, R.A., 2012. Deconvolving BOLD activation in event-related designs for multivoxel pattern classification analyses. NeuroImage 59, 2636–2643. doi:10.1016/j.neuroimage.2011.08.076.

[27] Nichols, T.E., Holmes, A.P., 2002. Nonparametric permutation tests for functional neuroimaging: a primer with examples. Human brain mapping 15, 1–25.

[28] Olivetti, E., Veeramachaneni, S., Nowakowska, E., 2012. Bayesian hypothesis testing for pattern discrimination in brain decoding. Pattern Recognition 45, 2075–2084. URL: https://linkinghub.elsevier.com/retrieve/pii/S0031320311001841, doi:10.1016/j.patcog.2011.04.025.

[29] Pernet, C.R., McAleer, P., Latinus, M., Gorgolewski, K.J., Charest, I., Bestelmeyer, P.E., Watson, R.H., Fleming, D., Crabbe, F.a., Valdes-Sosa, M., et al., 2015. The human voice areas: Spatial organization and inter-individual variability in temporal and extra-temporal cortices. Neuroimage 119, 164–174.

[30] Ryali, S., Supekar, K., Abrams, D.A., Menon, V., 2010. Sparse logistic regression for whole-brain classification of fmri data. NeuroImage 51, 752–764.

[31] Stelzer, J., Chen, Y., Turner, R., 2013. Statistical inference and multiple testing correction in classification-based multi-voxel pattern analysis (mvpa): random permutations and cluster size control. Neuroimage 65, 69–82.

[32] Takerkart, S., Auzias, G., Thirion, B., Ralaivola, L., 2014. Graph-based inter-subject pattern analysis of fMRI data. PloS ONE 9, e104586. doi:10.1371/journal.pone.0104586.

[33] Todd, M.T., Nystrom, L.E., Cohen, J.D., 2013. Confounds in multivariate pattern analysis: Theory and rule representation case study. NeuroImage 77, 157–165. doi:10.1016/j.neuroimage.2013.03.039. bibtex: todd_confounds_2013.

[34] Varoquaux, G., 2018. Cross-validation failure: Small sample sizes lead to large error bars. NeuroImage 180, 68–77. doi:10.1016/j.neuroimage.2017.06.061.

Inter-subject pattern analysis
A straightforward and powerful scheme for group-level MVPA

Qi Wang, Bastien Cagna, Thierry Chaminade, Sylvain Takerkart

https://doi.org/10.1016/j.neuroimage.2019.116205

Supplementary materials

1. Influence of the number of subjects and number of samples per subject

Aim. Although the two real fMRI datasets used in our experiments have approximately the same total number of observations (5400 observations in *Dataset1*, 5616 observations in *Dataset2*), they differ in the number of subjects that were scanned and the number of trials per subject: *Dataset1* includes 360 trials for each of the 15 subjects, while *Dataset2* offers 144 trials for 39 subjects. We here attempt to investigate whether this could explain some of the differences we observed in the results of G-MVPA and ISPA on these two datasets, using new artificial datasets.

Experiments. We therefore repeat the same set of experiments as in the paper, using new sets of 14300 datasets generated to maintain the size of the training set constant and modulating the ratio between the number of subjects S and the number of samples per subject N. We used the following parameter values: $(S, N) \in \{(9, 500), (11, 400), (17, 250), (21, 200), (51, 80), (101, 40), (201, 20), (401, 10)\}$, which allows maintaining the size of the group-level dataset approximately constant (and more particularly, the size of the ISPA training set is exactly constant at $(S - 1) \times N = 4000$).

Results. We present below the results we obtained, under the same summarized form as in Table 3 of the paper. Tables S1 to S8 represent the two-dimensional parameter space spanned by d and Θ, for various values of the (S, N) couple. The cells colored in blue are those where G-MVPA and ISPA yielded significant group-level decoding for 50 or more datasets out of the 100, whereas in the green cells it is the case only for G-MVPA and in the red ones it is the case only for ISPA.

The shape of the region where G-MVPA yields 50 or more significant detections, corresponding here to the green and blue cells, remains approximately rectangular for all values of (S, N). But when the number of subject S increases, it is shifted to the right of the table, i.e. G-MVPA is effective only for larger effect sizes. This is a direct consequence of the decreasing value of N, which is critical for within-subject decoding. For ISPA, the shape and location of the colored region (red and blue cells) where it is effective remains fairly constant, showing that ISPA is not or weakly affected by the ratio N/S when the size of the training set is constant.

We now try to address the question of whether the difference in the N/S ratio between *Dataset1* and *Dataset2* can explain the fact that the most peripheral regions of the main clusters are detected by ISPA for *Dataset1* and G-MVPA for *Dataset2*, in the light of the present results where we vary N/S in artificial datasets. The N/S ratio for *Dataset1* is $360/15 = 24$, while for *Dataset2*, it is $144/39 = 3.7$. We reformulate the previous question as follows: if the N/S ratio of *Dataset1* were smaller (i.e. closer to the one of *Dataset2*), could the peripheral voxels – which are red on Figure 5 of the paper, i.e. are detected by ISPA – *become* green, i.e. be detected only by G-MVPA? For this, consider a red cell in Table S3 (for which the N/S ratio is the closest to the one of *Dataset1*): can it become green when the ratio N/S decreases? We clearly see that it is not possible, i.e. that all red cells in Table S3 are also red (in almost all cases) in Tables S4 to S8 where N/S is smaller. We then ask the opposite question: if the N/S ratio of *Dataset2* were larger (i.e. closer to the one of *Dataset1*), could the peripheral voxels – which are green on Figure 5 of the paper, i.e. are detected by G-MVPA – *become* red, i.e. be detected only by ISPA? For this, consider a green cell in Table S5 (for which the N/S ratio is the closest to the one of *Dataset2*): can it become red when the ratio N/S increases? We clearly see that it is not possible, i.e. that all green cells in Table S5 are also green (in almost all cases) in Tables S1 to S4 where the N/S ratio is larger. This parallel between the real and the artificial datasets therefore suggests that it is not the difference of N/S ratio between *Dataset1* and *Dataset2* that can explain the different behaviors observed in the periphery of the significant clusters between G-MVPA and ISPA, illustrated on Figure 5 of the paper.

Table S1: Visual comparison of G-MVPA vs. ISPA, 9 subjects, 500 data points per subject

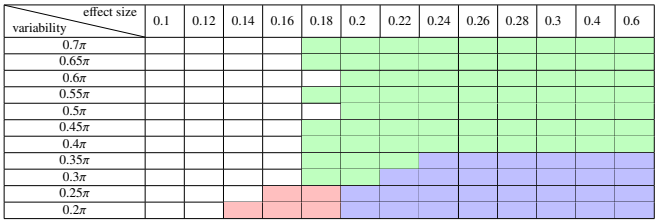

Table S2: Visual comparison of G-MVPA vs. ISPA, 11 subjects, 400 data points per subject

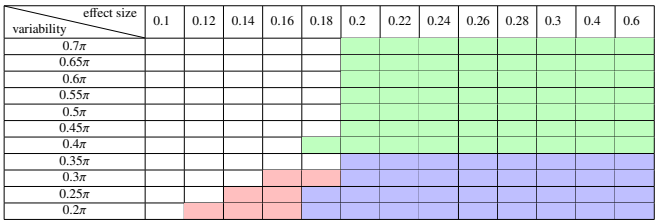

Table S3: Visual comparison of G-MVPA vs. ISPA, 17 subjects, 250 data points per subject

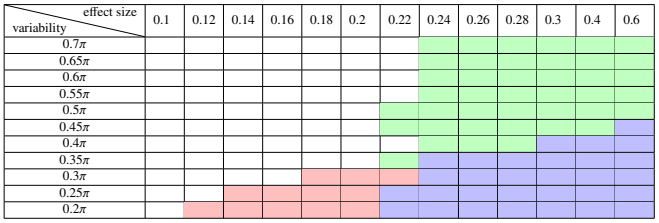

Table S4: Visual comparison of G-MVPA vs. ISPA, 21 subjects, 200 data points per subject

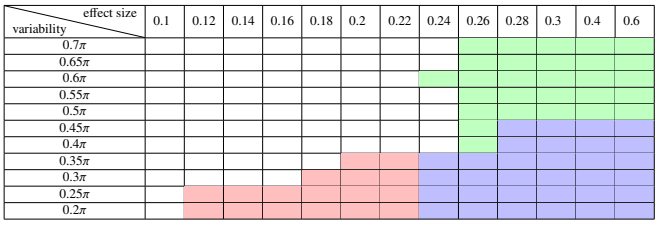

Table S5: Visual comparison of G-MVPA vs. ISPA, 51 subjects, 80 data points per subject

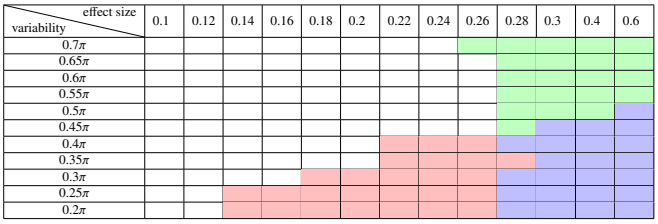

Table S6: Visual comparison of G-MVPA vs. ISPA, 101 subjects, 40 data points per subject

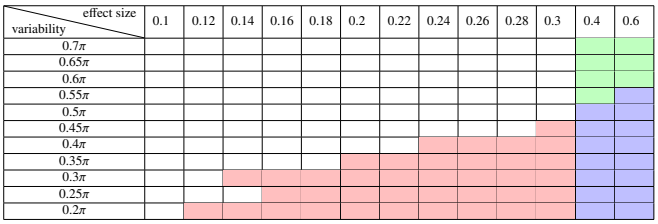

Table S7: Visual comparison of G-MVPA vs. ISPA, 201 subjects, 20 data points per subject

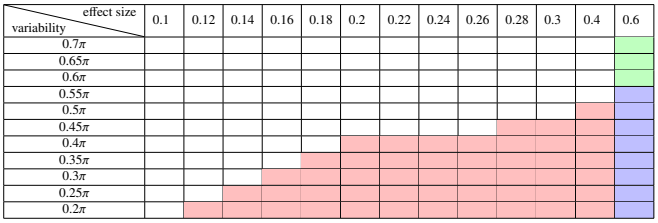

Table S8: Visual comparison of G-MVPA vs. ISPA, 401 subjects, 10 data points per subject

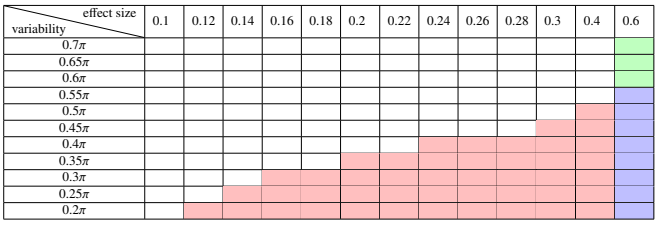

2. Influence of the within-subject covariance

Aim. Group-level decoding is strongly influenced by the ratio of the inter- and within-subject variance. To study the influence of this ratio, we performed experiments in the paper where the within-subject covariance Σ was fixed and the inter-subject variability was parametrically controlled, using our generative model to create a large number of artificial datasets. Here, we study whether our results hold when we change the within-subject variance.

Experiments. In this section we vary both the within- and inter-subject variability. We keep the same range of values for Θ, which controls the amount of inter-subject variability: $\Theta \in \{0.2\pi, 0.25\pi, 0.3\pi, 0.35\pi, 0.4\pi, 0.45\pi, 0.5\pi, 0.55\pi, 0.6\pi, 0.65\pi, 0.7\pi\}$. And we generate five new sets of 14300 datasets using five values for the within-subject covariance matrix: $\Sigma_1 = \begin{pmatrix} 1 & 0 \\ 0 & 5 \end{pmatrix}, \Sigma_2 = \begin{pmatrix} 3 & 0 \\ 0 & 5 \end{pmatrix}, \Sigma_3 = \begin{pmatrix} 5 & 0 \\ 0 & 5 \end{pmatrix}, \Sigma_4 = \begin{pmatrix} 7 & 0 \\ 0 & 5 \end{pmatrix}$, $\Sigma_5 = \begin{pmatrix} 9 & 0 \\ 0 & 5 \end{pmatrix}$. We fix the number of subjects to 21 and generate 200 data points for each subject. Figure S1 illustrates the effect of each of these five covariance matrices on the properties of the generated datasets, for $d = 2$ and $\Theta = 0$. In short, the distinctiveness of the two classes decreases from Σ_1 to Σ_5.

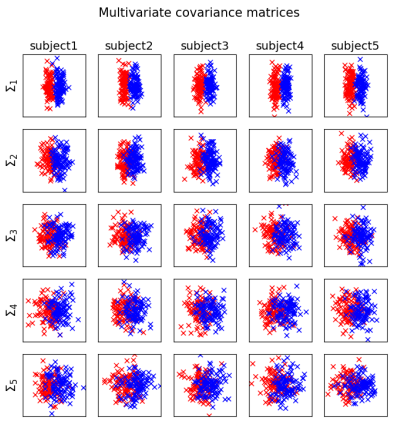

Figure S1: Illustration of the artificial datasets generated with five covariance matrices. Each line is a subpart of a single dataset (5 subjects shown amongst 21), $d = 2$ and $\Theta = 0$.

Results. Our results are shown in Tables S9 to S13. As previously, G-MVPA and ISPA yield more that 50 detections out of the 100 datasets available in each cell in regions that only partially overlap. Both strategies are strongly influenced by the within-subject covariance Σ, i.e. they prove less effective when going from Σ_1 to Σ_5, i.e. when the within-subject distinctiveness of the patterns decreases. However, the shape of the different regions in this parameter space remains constant: G-MVPA is effective in a rectangle area (blue + green cells), showing that it is not affected by the amount of inter-subject variability; and ISPA is effective in a triangle-like area (blue + red cells). This shows that the qualitative nature of our results does not seem to be affected by the value of Σ.

Table S9: Visual comparison of G-MVPA vs. ISPA, Σ_1

variability \ effect size	0.1	0.12	0.14	0.16	0.18	0.2	0.22	0.24	0.26	0.28	0.3	0.4	0.6
0.7π													
0.65π													
0.6π													
0.55π													
0.5π													
0.45π													
0.4π													
0.35π													
0.3π													
0.25π													
0.2π													

Table S10: Visual comparison of G-MVPA vs. ISPA, Σ_2

variability \ effect size	0.1	0.12	0.14	0.16	0.18	0.2	0.22	0.24	0.26	0.28	0.3	0.4	0.6
0.7π													
0.65π													
0.6π													
0.55π													
0.5π													
0.45π													
0.4π													
0.35π													
0.3π													
0.25π													
0.2π													

Table S11: Visual comparison of G-MVPA vs. ISPA, Σ_3

variability \ effect size	0.1	0.12	0.14	0.16	0.18	0.2	0.22	0.24	0.26	0.28	0.3	0.4	0.6
0.7π													
0.65π													
0.6π													
0.55π													
0.5π													
0.45π													
0.4π													
0.35π													
0.3π													
0.25π													
0.2π													

Table S12: Visual comparison of G-MVPA vs. ISPA, Σ_4

variability \ effect size	0.1	0.12	0.14	0.16	0.18	0.2	0.22	0.24	0.26	0.28	0.3	0.4	0.6
0.7π													
0.65π													
0.6π													
0.55π													
0.5π													
0.45π													
0.4π													
0.35π													
0.3π													
0.25π													
0.2π													

Table S13: Visual comparison of G-MVPA vs. ISPA, Σ_5

variability \ effect size	0.1	0.12	0.14	0.16	0.18	0.2	0.22	0.24	0.26	0.28	0.3	0.4	0.6
0.7π													
0.65π													
0.6π													
0.55π													
0.5π													
0.45π													
0.4π													
0.35π													
0.3π													
0.25π													
0.2π													

3. Influence of spatial smoothing on the results obtained on the real fMRI datasets

Aim. The preprocessing steps performed in the paper on the two fMRI datasets did not include any spatial smoothing. Since there is a debate in the literature on the validity and interest of such smoothing when performing MVPA, we here study the influence of the smoothing on our results.

Experiments. We replicate the same experiments as in the paper by adding some spatial smoothing on the beta maps that are used to construct the inputs of the classifier. We use the Gaussian kernel implemented in SPM to perform the smoothing, with full-width at half-maximum values of 3 mm and 6 mm.

Results. For clarity, we denote as *Dataset1-s3* and *Dataset2-s3* the versions of the two datasets with the 3 mm smoothing, and *Dataset1-s6* and *Dataset2-s6* with the 6 mm smoothing. The results are presented in the same way as in the paper for the unsmoothed data: Figure S2 and S3 show the thresholded statistical maps, displaying the significant clusters; Figure S4 and S5 present the analysis of the size of the main cluster and its peak statistic value, for each dataset, each hemisphere and each size of the searchlight radius; finally, Figure S6 and S7 describe how the main clusters obtained with G-MVPA and ISPA overlap.

Overall, the results obtained with smoothing are consistent with what we found with the unsmoothed data: clusters were found in the same regions of the brain, their size increased with the value of the searchlight radius and the patterns of overlap between the clusters found by G-MVPA and ISPA were overall similar.

The main effect of smoothing appears to be that the number of significant voxels increases when the size of the smoothing kernel increases, from 0 mm to 3 mm to 6 mm. This can be explained by the fact that a small amount of smoothing helps reduce noise which can slightly improve decoding accuracies on the one hand and also increase the reproducibility across cross-validation folds on the other hand. This therefore facilitates detection as probed by our statistical test on accuracies.

Furthermore, a notable difference observed with 6 mm smoothing is the fact that the size of the activated clusters found by ISPA for *Dataset2-s6* is as large as the ones found by G-MVPA, which is not the case with smaller or no smoothing (see bottom-left graph in Figure S5, compared with the one in Figure S4 or with Figure 4 in the paper). Congruently, the pattern of overlapping of the clusters found by the two strategies is modified for *Dataset2-s6* when compared with the one found with smaller or no smoothing (see the right graph of Figure S7, compared to the right graph on Figure S6 and Figure 6 in the paper): the number of voxels detected only by G-MVPA (green voxels) decreased in an important proportion. This is consistent with the putative explanation that was put forward in the paper, that stated that the large amount of green voxels found in *Dataset2* could be caused by a large inter-individual variability: indeed, one of the effect of spatial smoothing is often to reduce this inter-individual variability. In a complementary manner, this could also mean that the idiosyncrasies that could drive the detection of the green voxels leave at high spatial frequencies. The spatial smoothing, by attenuating these frequencies, would therefore make them vanish as we observe in this experiment.

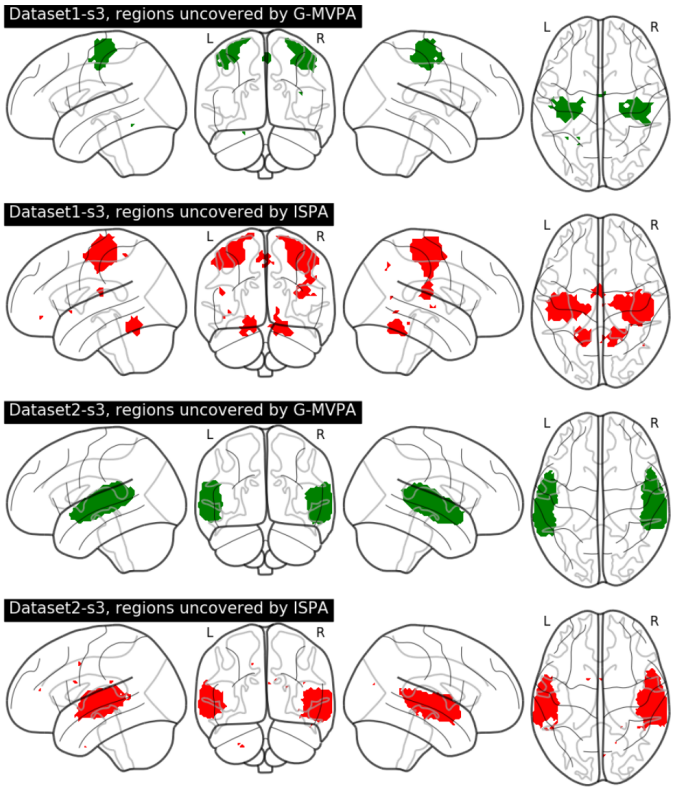

Figure S2: Illustration of the results of the group-level searchlight decoding analysis for a 6 mm radius with *Dataset1-s3* and *Dataset2-s3*. Top two rows: *Dataset1-s3*; bottom two rows: *Dataset2-s3*. Brain regions found significant using G-MVPA and ISPA are respectively depicted in green and red.

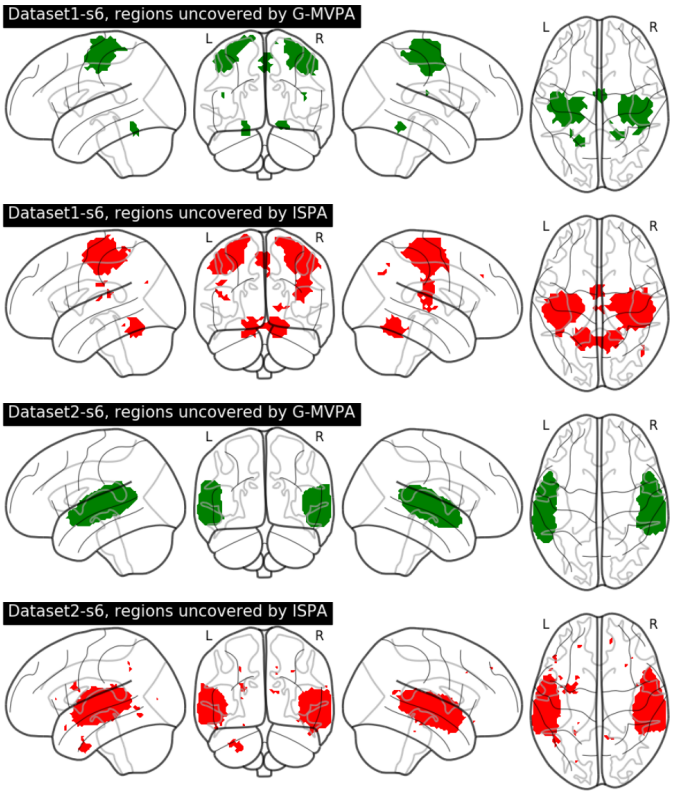

Figure S3: Illustration of the results of the group-level searchlight decoding analysis for a 6 mm radius with *Dataset1-s6* and *Dataset2-s6*. Top two rows: *Dataset1-s6*; bottom two rows: *Dataset2-s6*. Brain regions found significant using G-MVPA and ISPA are respectively depicted in green and red.

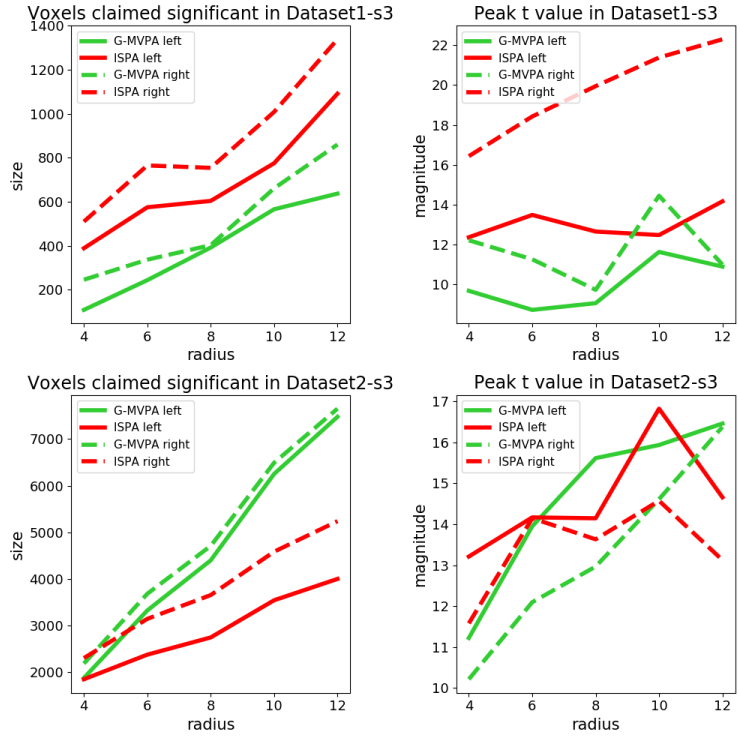

Figure S4: Quantitative evaluation of the results obtained on the smoothed fMRI datasets for G-MVPA (green curves) and ISPA (red curves), 3 mm Gaussian kernel. Solid and dashed lines for the largest cluster respectively in the left and right hemispheres. Left column: size of the significant clusters. Right column: peak *t* statistic. Top vs. bottom row: results for *Dataset1-s3* and *Dataset2-s3* respectively.

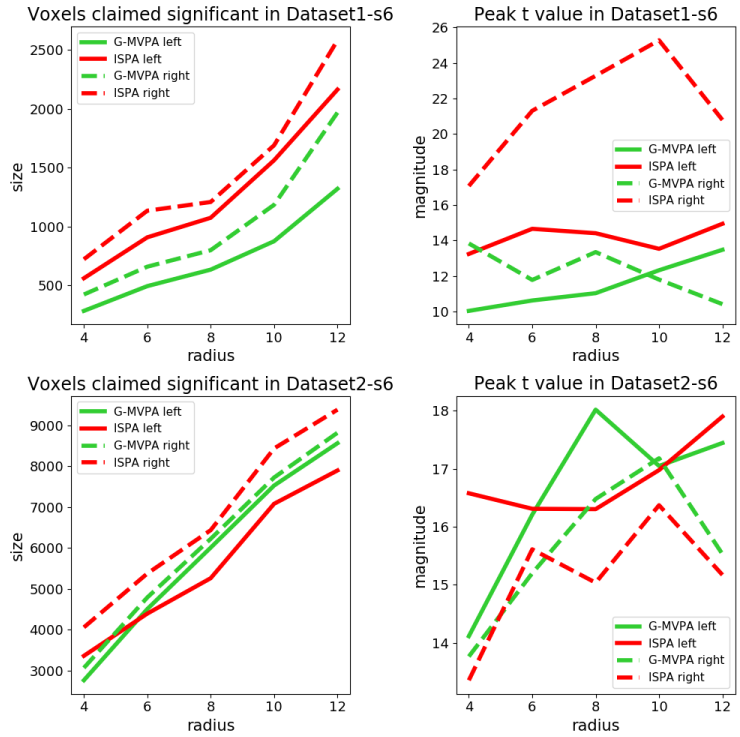

Figure S5: Quantitative evaluation of the results obtained on the smoothed fMRI datasets for G-MVPA (green curves) and ISPA (red curves), 6 mm Gaussian kernel. Solid and dashed lines for the largest cluster respectively in the left and right hemispheres. Left column: size of the significant clusters. Right column: peak *t* statistic. Top vs. bottom row: results for *Dataset1-s6* and *Dataset2-s6* respectively.

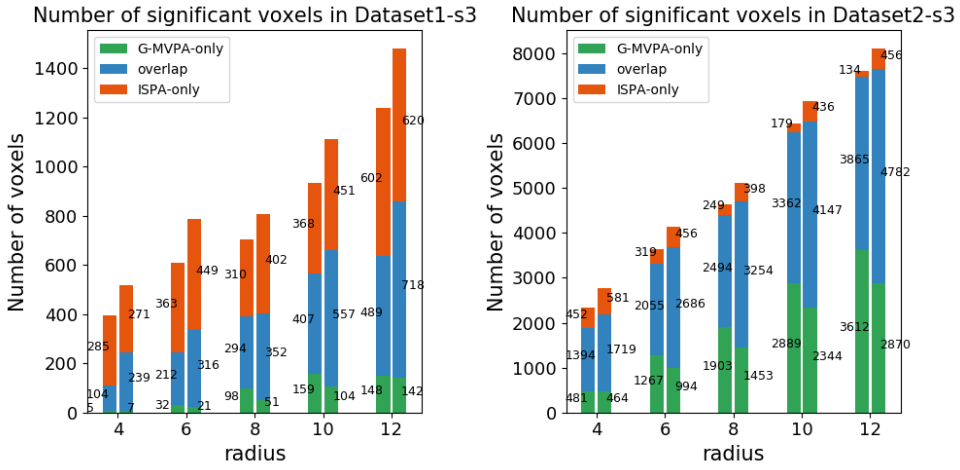

Figure S6: Comparison of the voxel counts detected by G-MVPA-only (green), ISPA-only (red) or both (blue) for the different values of the searchlight radius, in *Dataset1-s3* (left) and *Dataset2-s3* (right)

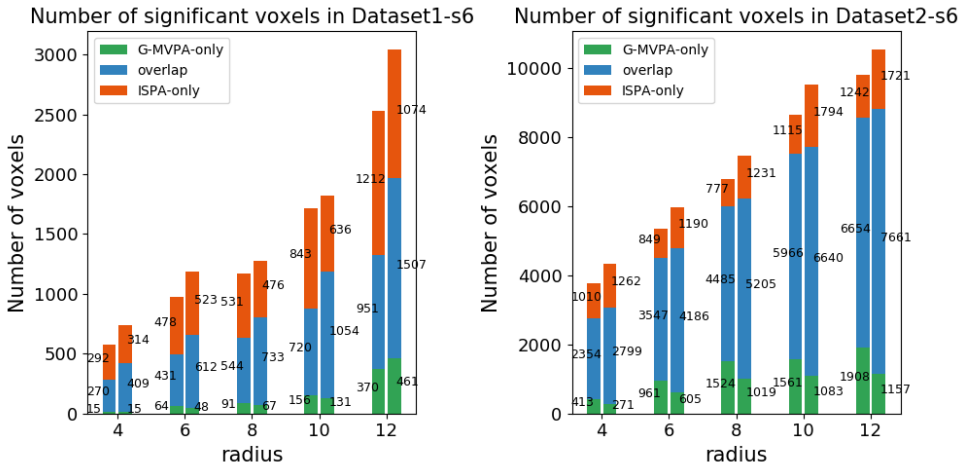

Figure S7: Comparison of the voxel counts detected by G-MVPA-only (green), ISPA-only (red) or both (blue) for the different values of the searchlight radius, in *Dataset1-s6* (left) and *Dataset2-s6* (right).

4. Bias and variance analyses for G-MVPA and ISPA

Aim. In order to further compare G-MVPA and ISPA, we here assess their bias and variance for estimating classifiers. For this, we exploit the generative model used to construct our artificial dataset to define the true classifier, and measure how each strategy deviates from this ground truth.

Experiments. In this section we use the same artificial datasets as in Section 2.3 of the paper. Before inducing some random inter-individual variability with a rotation around the origin, the two classes are separated by the the straight line $x = 0$. Because the mean variability (i.e. rotation angle) across the population is equal to zero, the true group-level classifier is defined by $f : x = 0$. Classifiers estimated from the i-th subject in G-MVPA or the i-th cross-validation split in ISPA are denoted as f_G^i and f_I^i, respectively. We use the angle between the estimated and true classifiers to measure the estimation error: the angles between f_G^i and f, f_I^i and f are denoted as θ_G^i and θ_I^i, respectively. We can then compute:

$$bias_G = \frac{1}{S}\sum_{i=1}^{i=S}\theta_G^i$$

$$var_G = \frac{1}{S}\sum_{i=1}^{i=S}(\theta_G^i - bias_G)^2$$

$$bias_I = \frac{1}{S}\sum_{i=1}^{i=S}\theta_I^i$$

$$var_I = \frac{1}{S}\sum_{i=1}^{i=S}(\theta_I^i - bias_I)^2$$

where $bias_G$, var_G and $bias_I$, var_I are the bias and variance of G-MVPA and ISPA respectively. For each point in the parameter space defined by d and Θ, we compute the average bias and variance of the 100 datasets available in each cell of the tables shown in Section 3.1 of the main paper.

Results. The values of the average bias and variance of G-MVPA and ISPA are shown as the intensities of the images presented on Figure S8, which represent the parameter space defined by d and Θ, as in Tables 1-3 of the main manuscript. Overall, the bias and variance of ISPA appears to be more constant than the ones of G-MVPA, which reach much higher values. ISPA leads to a smaller bias than G-MVPA everywhere, except in a limited part of the parameter space with large effect size and relatively low inter-subject variability, which corresponds to cases where both strategies provide equivalent detection power. Moreover, the variance of ISPA is smaller than the one of G-MVPA in all cases. In summary, ISPA present smaller bias and variance than G-MVPA in all the challenging part of the parameter space, i.e. where the effect size is small or the variability is large.

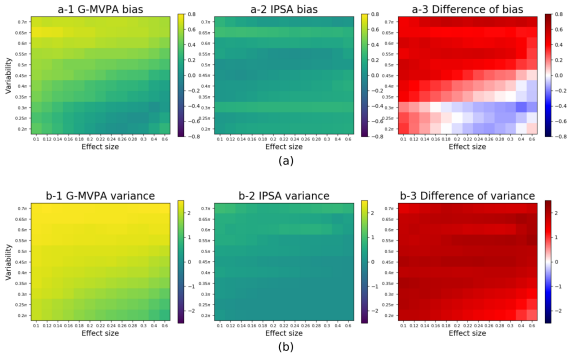

Figure S8: Results of the bias and variance analyses. Top, from left to right: bias of G-MVPA, bias of ISPA, difference $bias_G - bias_I$. Bottom, from left to right: variance of G-MVPA, variance of ISPA, difference $var_G - var_I$.

5. Assessing false positive rates in G-MVPA and ISPA

Aim. In order to complement the sensitivity analyses presented in the main manuscript, we here perform a specificity analysis by measuring the number of false positives produced by G-MVPA and ISPA on artificial data sets where the true effect size is null.

Experiments. We use the same generative model as in the paper, but we set d to zero, which allows obtaining datasets that contain no effect. Furthermore, we generate datasets with different amounts of inter-individual variability by choosing Θ in $\{0, 0.05\pi, 0.1\pi, 0.15\pi, 0.2\pi, 0.25\pi, 0.3\pi, 0.35\pi, 0.4\pi, 0.45\pi, 0.5\pi, 0.55\pi, 0.6\pi, 0.65\pi, 0.7\pi\}$. For each value of Θ, we generate 1000 independent datasets. The number of datasets for which group-level decoding accuracy is significant is counted using the procedure described in Section 2.6. Because there is no true effect, all these datasets are false positives. With a threshold set at $p < 0.05$ in the permutation test, we should obtain 5% false positives or less, i.e. 50 datasets at most.

Results. The numbers of false detections obtained with G-MVPA and ISPA are shown in Table S14. Overall, in all cases, both strategies detect an effect in more than 50 datasets out of 1000 whereas there is none. This indicates an inflated false positive rate (on average 6.4% for G-MVPA and 9.7% for ISPA) when the statistical inference is performed with a permutation test on accuracies.

Discussion. For G-MVPA, as already documented in the literature, this could be caused by the non-symmetric nature of the distribution of accuracies (which violate the exchangeability assumption of the permutation test), or by the lack of use of the uncertainty of single-level measurements (as addressed in (Olivetti et al., 2012)). Several solutions have been proposed, as mentioned in the main manuscript (Olivetti et al., 2012; Brodersen et al., 2013; Stelzer et al., 2013; Etzel, 2015; Allefeld et al., 2016). For ISPA, the same argument about the asymmetry of the distribution holds as a potential cause for this inflated rate of false positives. Furthermore, another potential cause might be the dependence between the accuracies measured on each fold: indeed, even though the test sets are totally independent between the different folds of a leave-one-subject-out cross-validation, the classifiers learnt on each fold are not independent because of the large amount of overlap between the training sets of each fold. To the best of our knowledge, no solution has been proposed in the neuroimaging literature to handle this specific question of statistical inference on inter-subject accuracies. A solution directly applicable could be to use label permutations on the observations (as in Stelzer et al., 2013). We did not use it because of the exponentially high computing time required for this, and also because we believe that these inflated positive rates observed for the two strategies do not question the nature of our results. Indeed, even if a few percents of the detections are mistagged as positives, i) the shape of Table 3 of the main manuscript (that summarizes the comparison of G-MVPA and ISPA on the artificial datasets) will hold, and ii) the qualitative assessment of the statistical maps obtained on real data would barely be affected because it is based on the largest clusters, which are clearly not false positives.

Table S14: Number of false positives obtained using the permutation test with G-MVPA and ISPA

variability	G-MVPA	ISPA
0.7π	62	80
0.65π	64	112
0.6π	69	100
0.55π	55	105
0.5π	62	98
0.45π	62	99
0.4π	70	92
0.35π	63	102
0.3π	57	89
0.25π	69	82
0.2π	56	98
0.15π	68	94
0.1π	62	98
0.05π	75	112
0π	71	95